HHS Public Access

Author manuscript

Anal Chem. Author manuscript; available in PMC 2018 March 07.

Published in final edited form as:

Anal Chem. 2017 March 07; 89(5): 2731–2738. doi:10.1021/acs.analchem.6b02377.

Structural Characterization of Native Proteins and Protein Complexes by Electron Ionization Dissociation-Mass Spectrometry

Huilin Li[†,*], **Yuewei Sheng**[#], **William McGee**[‡], **Michael Cammarata**[‡], **Dustin Holden**[‡], and **Joseph A. Loo**[†,#,*]

[†]Department of Biological Chemistry, David Geffen School of Medicine, University of California, Los Angeles, CA, 90095, United States

[#]Department of Chemistry and Biochemistry, UCLA/DOE Institute of Genomics and Proteomics, and UCLA Molecular Biology Institute, University of California, Los Angeles, CA, 90095, United States

[‡]Department of Chemistry, The University of Texas at Austin, Austin, Texas 78712, United States

Abstract

Mass spectrometry (MS) has played an increasingly important role in the identification and structural and functional characterization of proteins. In particular, the use of tandem mass spectrometry has afforded one of the most versatile methods to acquire structural information for proteins and protein complexes. The unique nature of electron capture dissociation (ECD) for cleaving protein backbone bonds while preserving non-covalent interactions has made it especially suitable for the study of native protein structures. However, the intra- and inter-molecular interactions stabilized by hydrogen bonds and salt bridges can hinder the separation of fragments even with pre-activation, which has become particularly problematic for the study of large macromolecular proteins and protein complexes. Here, we describe the capabilities of another activation method, 30 eV electron ionization dissociation (EID), for the top-down MS characterization of native protein-ligand and protein-protein complexes. Rich structural information that cannot be delivered by ECD can be generated by EID. EID allowed for the comparison of the gas-phase and the solution-phase structural stability and unfolding process of human carbonic anhydrase I (HCA-I). In addition, the EID fragmentation patterns reflect the structural similarities and differences among apo-, Zn-, and Cu,Zn-superoxide dismutase (SOD1) dimers. In particular, the structural changes due to Cu-binding and a point mutation (G41D) were revealed by EID-MS. The performance of EID was also compared to that of 193 nm ultraviolet photodissociation (UVPD), which allowed us to explore their qualitative similarities and differences as potential valuable tools for the MS study of native proteins and protein complexes.

Graphical abstract

[*]Corresponding Authors: lihuilin@gmail.com (H. Li); JLoo@chem.ucla.edu (J.A. Loo).

Notes: The authors declare no competing financial interest.

Associated Concent Supporting Information: The Supporting Information is available free of charge via the Internet at http://pubs.acs.org.

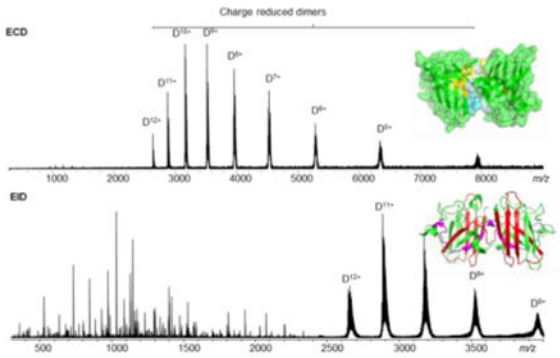

Introduction

Proteins are versatile biomolecules in living systems, and the structures of proteins and protein complexes determine their biological functions. How proteins function and how they assemble into functional macromolecular complexes remain as some of the most puzzling questions in molecular life sciences. Thus, the structural and functional characterization of proteins can contribute towards our understanding of their biological processes at the molecular level. As a complementary method to more conventional technologies used in structural biology, such as nuclear magnetic resonance spectroscopy, X-ray crystallography, and electron microscopy, native mass spectrometry (native MS) with electrospray ionization (ESI) has established its growing role in the characterization of noncovalently-bound protein complexes, revealing the composition, stoichiometry, dynamics, stability, and spatial arrangements of subunits in protein assemblies in a sensitive and rapid manner[1-4].

The utility of tandem mass spectrometry (MS/MS) to derive structural information from large proteins and protein complexes has been demonstrated. Several categories of activation/dissociation techniques have been used for such analysis, including collisional-based dissociation (collisionally activated dissociation (CAD)[5], surface induced dissociation (SID)[6], electron-based dissociation (electron capture dissociation (ECD)[7, 8], electron transfer dissociation (ETD)[9], and photon-based dissociation techniques (infrared multiphoton dissociation (IRMPD)[10, 11] and ultraviolet photodissociation (UVPD))[12, 13]. ECD is especially powerful, cleaving protein backbone bonds while retaining non-covalent interactions for the subsequent measurement by MS, which therefore makes the study of proteins and protein-ligand interactions feasible under native solution conditions[14-16].

Despite the fact that several groups have demonstrated that structurally relevant information can be obtained with a single top-down ECD or a similar technique ETD experiment for protein complexes[8-10, 17, 18], there are several challenges associated with the nature of ECD/ETD when facing *native* protein complexes. First, the electron capture efficiency and fragmentation efficiency are charge dependent[19]. Ions from folded native proteins and protein complexes carry much fewer charges compared to their denatured counterparts. Thus, the ECD/ETD efficiency and the resulting information for a protein or a protein complex with lower charge states will suffer in comparison with that of the same protein under denaturing solution conditions. Second, the capture of low energy electrons during

ECD or the transfer of low electrons from anions to protein cations during ETD results in the formation of odd-electron radical species with little vibrational energy redistribution prior to the cleavage of N-C_α backbone bonds, thus preserving labile posttranslational modifications and noncovalent interactions[7]. But the intra- and inter-molecular interactions stabilized by hydrogen bonds or salt bridges can hinder the separation of fragments, which can be particularly problematic for the study of proteins or protein complexes under native condition[20]. The further development of newer activation/dissociation techniques is therefore needed, particularly for the efficient characterization of native protein complexes to derive information, not only on their primary sequences, but also modifications and higher order structures.

Over the past few years, one activation technique in particular, UVPD using 193 nm radiation (in the vacuum UV region) developed by the Brodbelt group has attracted much attention, as it can cope with many of the challenges faced by other methods and has been shown to be a valuable technique for deriving structural information of native proteins and protein complexes[21-26]. A single 193 nm photon deposits 6.4 eV of energy, which is sufficient to cause dissociation by directly accessing excited electronic states, leading to a diversity of fragmentation pathways (e.g., a/b/c- and x/y/z-product ions)[12]. Extensive sequence information with retention of labile modifications and non-covalent ligand-bound fragment ions has been observed[22, 24, 26]. Sequence coverage for native and denatured proteins by UVPD was found to be independent of the charge state of the precursor ions[12]. Non-covalently bound protein-protein product ions have also been detected, which is useful tertiary and quaternary structure information[22]. Even for native proteins with compact gas-phase structures, such as ubiquitin, myoglobin, cytochrome C, etc., sequence information and ligand-binding sites have been revealed[22, 24].

Based on criteria such as the form in which energy is deposited (electronic or vibrational), the time over which activation occurs, the amount of energy that can be deposited into the ion, etc., activation methods can be divided into two categories, slow activation methods and fast activation methods[27]. Slow activation methods such as CAD and IRMPD deposit energy to the vibrational states through multiple collisions or multiple photon absorption, and the times between activation events can be long relative to time frames for unimolecular chemistry, on the order of microseconds or longer. Activation events such as UVPD take place faster than the time frame of a vibrational period and directly deposit energy to an excited electronic state and can lead to different fragmentation behavior. Electron ionization dissociation (EID), introduced by Zubarev in 2009, is also a fast activation method[28] that appears to exhibit similar features to UVPD. In EID, the interaction of cation protein or peptide ions with > 20 eV electrons causes simultaneous ionization and electronic excitation of protein species to form electronically excited oxidized radical species, and subsequent fragmentation of the radical ions can yield the full complement of a/b/c- and x/y/z-product ions[28]. There are several attractive features associated with EID in comparison to ECD. Cations are oxidized rather than reduced during EID, which introduces different fragmentation channels to improve sequence yield. Another attractive feature is its capability to dissociate folded gas-phase proteins that are difficult to dissociate by ECD, suggesting that EID can separate fragment ions stabilized by noncovalent interactions from native proteins or protein complexes. To date, the capability of EID for native top-down MS has not

yet been fully explored. Here, by choosing a well characterized protein with a compact structure, carbonic anhydrase, and the superoxide dismutase protein dimer, we describe the capability of EID for the structural characterization of native proteins and protein-protein complexes. In addition, we compare the qualitative similarities and differences between EID and UVPD for native top-down MS.

Experimental Methods

Materials and Proteins

Carbonic anhydrase I from human (HCA-I) was purchased from Sigma (St. Louis, MO). The expression and purification of human superoxide dismutase-1 (SOD1), including the wild type (WT) in their apo-, Zn-bound, and Cu,Zn-bound forms and a mutant (G41D), were performed as described previously[29].

Sample Preparation

All proteins were dissolved in MilliQ water to a concentration of 100 μM, and then buffer exchanged three times with 200 mM ammonium acetate solution (300 μL each time) using Amicon centrifugal filters (Millipore Inc., Billerica, MA) with a molecular weight cut-off (MWCO) of 10 K. The buffer exchanged protein samples were then diluted with 200 mM ammonium acetate solution to a protein concentration of 3 μM for native nano-ESI-MS analysis.

Mass Spectrometry

FT-ICR MS—Protein solutions were loaded into metal-coated borosilicate capillaries (Au/Pd-coated, 1 μm I.D.; Thermo Fisher Scientific, West Palm Beach, FL) and electrosprayed at a flow rate of 10 - 40 nL/min through a nanospray ion source. The experiments were performed using a 15-T Bruker SolariX FTICR MS with an infinity cell. The ESI capillary voltage was set to 0.9-1.2 kV. The temperature of the drying gas was 80°C and the gas flow rate was 2.5 L/min. The RF amplitude of the ion-funnels was 300 V_{pp}, and the applied voltages were 200 V and 6 V for funnels 1 and 2, respectively. Skimmer 1 was varied up to 200 V to pre-heat ions but without inducing fragmentation and the skimmer 2 voltage was kept at 20 V. The lowest values of RF frequencies were used in all ion-transmission regions: multipole 1 (2 MHz), quadrupole (1.4 MHz), and transfer hexpole (2 MHz). Ions were accumulated for 500 ms in the hexapole collision cell before being transmitted to the infinity ICR cell. A time-of-flight of 1.5 ms was used. For the MS/MS experiments, the overall charge envelopes, 9+~11+ for HCA-I (Fig. S-1) and 10~12+ for SOD1 (Fig. S-2) were fragmented to avoid the significant ion-intensity-loss due to isolation. ECD experiments were performed with an ECD pulse length of 0.02 s, ECD bias of 1.5 V, and ECD lens of 15 V. EID experiments were performed with an ECD bias of 30V and all other parameters were kept the same. The ECD hollow-cathode current was 1.6 A. Two hundred scans were averaged for each spectrum and each experiment was performed in triplicate (n=3). Experiments were also repeated over time and mass spectra of equivalent quality were obtained with minimal tuning. All spectra were externally calibrated with cesium iodide.

Orbitrap MS—UVPD experiments were performed on a modified Thermo Scientific Orbitrap Elite mass spectrometer (Bremen, Germany) to accommodate an ArF 193 nm excimer laser (Coherent Existar XS) as described previously.[21] One or two pulses at 2.5 mJ per pulse was used for the UVPD experiments. All spectra were acquired at a resolving power of 240,000 with an average of 100 scans.

Data Processing

FTICR MS Data was processed in DataAnalysis (Bruker) and interpreted manually, fragment ion types including a- (a, a+2H), b-, c-, x-, y (y, y-2H)-, and z- were observed. Orbitrap spectra were interpreted using ProSight Lite and ions were matched against all available types of ions including a- (a, a+1), b-, c-, x- (x, x+1), y- (y, y-1), and z- ions. In addition, the presence of a+2H and y-2H ions was checked manually as they were not considered in ProSight Lite. The “sequence coverage” represents the percentage of the protein's sequence represented by the residues identified in the MS/MS. The backbone cleavages were calculated based on the total number of observed non-redundant backbone cleavages in the protein. Both of these parameters were taken into account when comparing EID and UVPD.

Results and Discussion

Carbonic Anhydrase

Carbonic anhydrase (CA) catalyzes the rapid inter-conversion of carbon dioxide and water to bicarbonate and protons. The active site of human carbonic anhydrase I (HCA-I) contains a zinc ion, located in the center of the structure and coordinating three histidine residues (His94, His96, and His119) (Fig. S-1A). HCA-I polypeptide predominantly forms a compact structure dominated by β-sheets and shows up at *m/z* 2,600 ~ 3,400 (11+~ 9+) under native ESI condition (Fig. S-1B). ECD of HCA-I (11+~9+) yielded no detectable c-/z-type ions; using more energetic in-source dissociation (ISD, 160V) yielded only a few z-ions of low intensity (**data not shown**). In contrast, higher energy EID of HCA-I provides sequence information without the need to pre-activate protein ions (Fig. 1A); however, more structure information was obtained by pre-activation of the ions using ISD. The EID backbone cleavage sites under different pre-activation conditions are plotted in Fig. S-1C. Overall the sequence coverage from EID was improved from 8% with 16 backbone cleavages to 50% with 47 backbone cleavages by increasing the ISD energy from 0 to 160 V (Fig. 1B), with all fragments originating from the C-terminal region.

CAs are a class of well-characterized proteins whose structural stabilities and folding/unfolding processes have been extensively studied[30-34]. Although HCA-I, HCA-II, and bovine CA-II share similar 3-D structures, their stabilities differ, with HCA-I having the most stable structure[35, 36]. Detailed studies using different approaches have demonstrated that the folding/unfolding process of HCA-II is reversible and proceeds in two stages[32, 33, 39]. The initiation of folding is indicated by a rapid collapse of a large hydrophobic cluster comprising the apolar residues on β-strands 2-6 and on the helix-containing segment between residues 220-242, followed by the folding of the C-terminal region, and then the N-terminal region[30, 31, 37]. The hydrophobic region encompassing β-

strands 3-5 appears to be remarkably stable and cannot be totally ruptured until extremely strong denaturing conditions are applied[38]. Hydrogen/deuterium (H/D) exchange results indicated that the N- and C-termini are flexible and truncation experiments demonstrated that the N-terminal residues interact favorably with the rest of the structure[30].

In view of the unfolding process of HCA-I, the gas phase molecule, especially the C-terminal region, appears to share similar features to the unfolding process of HCA-II in solution (Fig. 1B&C). EID of HCA-I readily yielded fragments from the C-terminal region (residues 242-260, as shown in yellow in Fig. 1C) without pre-activation; increasing ISD pre-activation from 0 to 60 V made no improvement in unfolding HCA-I, as indicated by the backbone cleavage yields. Further increasing ISD pre-activation to 80 V improved the sequence coverage, and even more so when increasing ISD pre-activation further to 120 V (Fig. 1B), which gradually unfolded the C-terminal regions from the residues 220-242 (in cyan) through residues 174-194 (in orange) and up to β-strand 6 (in green) as shown in Fig. 1C. Increasing ISD above 120 V made little difference in the fragmentation yield, which is consistent with the extreme stability of the hydrophobic core (β-strands 2-5) as observed in the unfolding process of CA in solution. In contrast, no fragments from the N-terminal region were observed. The lack of positive charge-carrying sites at the N-terminus might contribute to the absence of N-terminal fragments; there are only two potential charge-carrying sites for the first 20 amino acid residues from the N-terminus (K10 and K18) in comparison to five out of 20 residues at the C-terminal end. Another possible reason could be due to the interaction between the N-terminal amino acid residues with the rest of the structure[30], which forms strong hydrogen-bond and salt-bridge networks and causes difficulty for separating N-terminal fragments from the rest of the structure.

Superoxide Dismutase

Cu-Zn superoxide dismutase (SOD1) is a highly conserved enzyme that is the primary cytoplasmic scavenger of superoxide radicals. Human SOD1 is a 32 kDa homodimer protein in which each monomer consists primarily of an eight-stranded β-barrel with two large loops, the electrostatic loop (residue 122-143) and the metal binding loop (residue 49-84). Each SOD1 monomer also contains two metal ions, one copper and one zinc. The catalytic copper is bound by four histidine residues (His 46, 48, 63 and 120), and the zinc ion is bound by three histidine residues (His 63, 71, 80) and Asp 83 (Fig. S-3). A conserved disulfide bond between residues 57 and 146 greatly increases SOD1 stability.

The SOD1 homodimer protein is very sensitive to a variety of slow heating methods (e.g., ISD, CAD, IRMPD) and can be easily broken into monomers. To keep the dimer in its intact form, the parameters of the instrument were tuned to maintain a gentle ionization and transmission conditions and no pre-activation was applied for both ECD and EID experiments. The ECD and EID fragmentation behaviors of the apo-WT SOD1 dimer were compared (Fig. 2). ECD of apo-SOD1 dimer (10+ ~ 12+) yields only charge-reduced species without typical c-/z-type fragment ions, likely due to the involvement of both N- and C-termini with the interaction interfaces (residues 5-9, 17, 19, 49-54 from the N-terminus and residues 111-115, 148-153 from the C-terminus), according to calculations using PISA (Fig. 2A) (http://www.ebi.ac.uk/pdbe/prot_int/pistart.html). In contrast, EID yields fragment

ions from both termini with 50% sequence coverage (Fig. 2B). The charge-reduced/oxidized *dimers* found in the higher *m/z* region (rather than monomers) suggest that the fragment ions originate directly from these dimer species rather than from the monomers. In addition, the EID fragments are from the N- and C-terminal regions that directly participate in the subunit interaction interface, which suggests that the excessive energy deposited during EID goes into vibrational channels and leads to the separation of fragment ions bounded by noncovalent interactions. It is also consistent with the fact that EID backbone cleavages take place much faster than the time frame of a vibrational period. Monomers (7+) from the dissociation of SOD1 dimers were only observed as a minor process with a signal-to-noise level of 3.

To explore the ability of EID to reveal structural changes upon metal binding, the EID fragmentation mass spectra were compared for the apo-, Zn-, and Cu/Zn-bound forms of the WT-SOD1 dimers. The metal-binding states of the various forms of SOD1s were checked by applying ISD to remove salt adducts for subsequent ESI-MS (Fig. S-4). The fragmentation patterns for the three SOD1 forms share great similarity, which is consistent with their crystal structures (Fig. 3A). However, subtle differences due to metal-binding were observed, as indicated by the fragmentation patterns around residues 40-65 (Fig. 3B). To better display the structural differences, only the partial structure between residues 40 to 85 of each SOD1 monomer form is shown in Fig. 3C-E, which covers both the EID fragmentation region and the Cu/Zn binding regions. For apo-SOD1, the EID-induced backbone cleavage proceeded up to residue 54 (Fig. 3C). The binding of Zn^{2+} at His63, His71, His80, and Asp83 only appears to alter the local structure (residue 40-65) slightly that allows the EID backbone cleavage to reach to residue 64 (Fig. 3D). When Cu^{2+} binds to His46, His48, His63, and His120 (Fig. 3E), EID backbone cleavage stopped at residue 44. The conformation of the functional Loops IV (Cu^{2+} binding region) and VII (electrostatic loop) are less rigid in the absence of bound metals[39], and it has been proposed that metal binding is important for shielding the charged residues in Loops IV and VII to facilitate close packing with the β-barrel core[40]. It therefore explains the difficulty to liberate EID product ions from Cu/Zn-bound SOD1 to obtain sequence and metal-binding site information.

Interestingly, the differences among apo-, Zn-, and Cu/Zn-bound SOD1s were also reflected by the charge states of their fragment ions. The sites that provide positive charges can be tracked based on the charge states of the fragment ions (Fig. S-5). His46, the Cu^{2+}-binding site, provides a positive charge. The binding of Cu^{2+} ion to His46 does not only alter the ability of His46 to carry a positive charge but also makes the liberation of product ions difficult. The fragmentation of Cu/Zn-SOD1 therefore terminates at residue 44 with a maximum charge of 3+ (Fig. S-5C). However, the fragmentation patterns of the apo- and Zn-bound SOD1s extend beyond residue 44 and the product ions observed show a maximum charge of 4+ (Fig. S-5A&B).

Mutations to the SOD1 protein are a common link to familial amyotrophic lateral sclerosis (fALS). A major hypothesis in the field of ALS research is that SOD1 mutations decrease protein stability, alter protein folding and metal binding, and/or cause changes in other biophysical properties of the protein, resulting in an increased propensity of mutant SOD1 to

form neurotoxic aggregates[41]. In a study of ALS-mutant SOD1 amyloid fibrils by Chan et al., it was found that the first 63 N-terminal residues are involved in fibril formation[42]. Although the extended β-sheet of fibrils is largely stabilized by the hydrogen-bonding network of the polypeptide backbone, the residues' side-chains also can participate in hydrogen bonds and contribute to fibril stability. The packing of the β-sheet is sequence dependent. Substitutions at positions 37 or 41 with charged residues (G37R, G41D) significantly lower the twist distances within the fibrils. Intriguingly, both of the two mutants (G37R and G41D) cause a net change in charge in solution[42]. Tools that could monitor structural changes in SOD1 due to the binding of metal ions or the introduction of mutations would be valuable to further our understanding of the link between protein structure and pathogenesis.

To explore whether such subtle structural changes due to a point-mutation can be captured in the gas phase, WT and G41D SOD1 were obtained by EID-MS. Fig. 4 displays the charge states of all EID fragments along its backbone for the Zn-bound WT and G41D dimers. G41D substitution in Zn-SOD1 appears to prevent cleavage beyond residue 45 and no 4+ fragment ions were therefore observed (Fig. 4B). Although we did observe individual fragment-ion variations due to low peak intensity, such as c_{46}^{3+}, c_{54}^{4+}, and c_{64}^{4+} for Zn-SOD1 and c_{43}^{3+} and c_{44}^{3+} for Zn-G41D, the overall trends never changed in replicate measurements. It is reasonable to postulate that the introduction of a negative charge by substituting Gly with Asp at residue 41 might alter the local salt-bridge and hydrogen interaction networks in both solution and gas phase structures. Based on the similarity of the fragmentation patterns between Cu,Zn-SOD1 (Fig. S-5C) and Zn-bound G41D SOD1 (Fig. 4B), G41D substitution might have altered the protonated states of His-residues (His43 and/or His 46).

EID *versus* UVPD

Because the utility of UVPD for native top-down MS has recently been demonstrated[21-26], a qualitative comparison with EID would be useful to the field. EID's fragment-ion types (a/x, b/y, and c/z) and its capability for dissociating proteins and protein complexes of compact structures suggest that EID and UVPD might share some similarities. Therefore, to have a better understanding of their mechanisms and utilities, native top-down UVPD-MS analyses of HCA-I and SOD1s were performed and compared with results from EID-MS (albeit using two different instrument platforms).

UVPD experiments with 193 nm radiation were performed for using a modified Orbitrap mass spectrometer (UVPD experiments undertaken in the Brodbelt group at the University of Texas at Austin). For HCA-I, UVPD appeared to outperform EID and yielded 100% sequence coverage with 91 backbone cleavages from both N- and C-termini (compared to ca. 50% with 47 backbone cleavages for EID) (Fig. S-1C). The EID and UVPD fragmentation patterns at the N-terminal region of HCA-I were quite different, with fragment ions from the N-terminal observed in UVPD (represented by the red bar at the bottom of Fig. S-1C) but not in EID. Such difference is likely due to a combination of the differences in the fragmentation mechanism and energy level. EID process is charge-dependent, but UVPD shows less dependence on precursor ion charge states[12]; the lack of

positive charge-carrying sites at the N-terminal of HCA-I may consequently affect EID fragmentation but not that of UVPD. Moreover, the amount of energy deposited by EID and UVPD appears different. Backbone cleavages beyond the first 20 residues from the N-terminus were also observed in UVPD but not in EID, indicating that UVPD may be a higher energy activation process. Such indication was also reflected by the dissociation pattern of HCA-I at the C-terminal region. Although the UVPD backbone cleavage sites at the C-terminal region of HCA-I are largely in line with the ISD-EID results, unfolding of the HCA-I structure prior to UVPD dissociation through collisions was not needed. Moreover, UVPD of apo-SOD1 yields similar sequence coverage and backbone cleavage sites as EID but the level of dissociation of SOD1 dimer into monomers is significantly higher (Fig. S-6).

Although such disruption of the noncovalent interactions of native complexes has been frequently observed in UVPD studies[22, 43], it raises the question of whether sequence ions occur (i) directly from the complex precursors, (ii) via secondary dissociation of the folded sub-complexes, or (iii) via secondary dissociation of the unfolded monomers released by a CAD-type pathway. A detailed study by Morrison and Brodbelt suggested that UVPD may allow simultaneous access to higher energy pathways from disruption of the noncovalent interactions of the complexes and cleavage of protein backbone bonds to generate sequence ions, and thus sequence ions can occur through both (i) and (ii) pathways[43]. In contrast, EID consistently show higher degree of preservation of higher order structures than UVPD. Sequence ions from the SOD1 dimers by EID likely originate directly from the dimer radicals rather than via secondary dissociation of monomers. As the EID and UVPD experiments were performed on two different instruments (FT-ICR vs Orbitrap), the amount of pre-activation experienced by ions prior to UVPD or EID activation were likely different. A systematic one-on-one comparison between UVPD and EID on the same instrument platform would be ideal to eliminate such factors and to have a better comparison of their performance.

To further compare UVPD and EID, the backbone cleavages based on fragment ion-types are plotted as shown in Fig. 5. Fig. 5A and 5B displays the ISD(120V)-EID and UVPD fragmentation patterns of HCA-I, respectively. Likewise, Fig. 5C and 5D show EID and UVPD fragmentation patterns of apo-WT SOD1 dimer, respectively. The subtypes of each fragment-ion-type such as a, a+1, a+2, x, x+1, y, y-1, and y-2 were grouped together and displayed as a-/x-, b-/y- and c-/z-type of ions in Fig. 5. Overall, the regions from where product ions originated are rather similar between the two activation techniques. However, EID produces mostly c/z ions, with a/x and b/y ions only observed at the termini; UVPD yields predominantly a/x ions, followed by c/z and b/y ions. In addition, a+1, x+1, and y-1 ions are unique to UVPD. The differences observed in fragment-ion-types between EID and UVPD are due to their different dissociation mechanisms and pathways. The mechanism of UVPD is thought to involve photolytic radical cleavage of the C-Cα bond prior to elimination of the radical to generate a/x-ions and other subsequent products[44-46], whereas EID is a combination of double ionization followed by electron capture, ECD and EIEIO (electron-induced excitation in organics)[28]. The generation of a/x fragments is dominated by the cleavage of C_α-C bonds of hydrogen-deficient radicals (charge-oxidized species) and c/z ions are from the cleavage of N–C_α bonds of hydrogen-abundant radicals (charge-reduced species)[47]. It is therefore possible to increase the yield of charge-oxidized radicals and

subsequent a/x fragments by adjusting electron energy, which could be particularly useful for proteins that lack of charge sites at their termini, such as HCA-I.

Conclusions

Taking the compact protein HCA-I and protein complex SOD1s as examples, we demonstrate the utility of EID-MS for studying protein structures. Structural information beyond the primary sequence was obtained by EID and allowed us to compare the structural similarities and differences among different SOD1s and the unfolding processes of HCA-I in both gas and solution phases.

Based on the results from our study and the literature, UVPD appears to be a more efficient dissociation technique and is better suited for delivering structural information of proteins or protein complexes; however, electron-based dissociation techniques have their own unique features. The application of EID for the study of native proteins and protein complexes is still in its early stages. ECD (1.5 eV) and EID (30 eV) can be performed using the same electron gun without instrument modification and the information obtained from ECD and EID are complementary. From the SOD1 example, ECD yielded no fragments, which suggests the involvement of N-and C-termini in intra- or inter-subunit interactions (both N- and C-termini are involved in the subunit interaction interface), whereas EID provided direct sequence information of both termini by breaking the interaction interface. The information from ECD and EID together would be useful constraints for improving integrative modeling of low resolution structures from, for example, small angle X-ray scattering (SAXS) and cryo-electron microscopy (cryo-EM) to achieve near-atomic resolution.

The specific mechanistic details of EID and its potential to deliver structural information should be explored at different energy levels for macromolecular complexes of different molecular weights and stoichiometries. Although 30 eV electrons were used in our EID experiments, higher electron energy can be deposited using the same electron gun. Previously, such experiments were demonstrated by Zubarev's group[48]. Because different energy levels are likely to promote different dissociation pathways[47-50], future studies to explore higher electron energy-levels could extend the utility of EID or similar techniques for the structural study of macromolecular complexes.

Supplementary Material

Refer to Web version on PubMed Central for supplementary material.

Acknowledgments

Support from the US National Institutes of Health (R01 GM103479 and S10 RR028893 to JAL), the US Department of Energy (UCLA/DOE Institute for Genomics and Proteomics; DE-FC03-02ER63421), and the American Society for Mass Spectrometry (ASMS) Postdoctoral Research Award (to HL) are acknowledged. The UVPD-MS experiments were undertaken in the lab of Jennifer S. Brodbelt (University of Texas at Austin).

References

1. Heck AJR. Nat Meth. 2008; 5:927–933.
2. Heuvel, RHHvd, Heck, AJR. Curr Opin Chem Biol. 2004; 8:519–526. [PubMed: 15450495]

3. Sharon M, Horovitz A. Curr Opin Struct Biol. 2015; 34:7–16. [PubMed: 26005781]
4. Walzthoeni T, Leitner A, Stengel F, Aebersold R. Curr Opin Struct Biol. 2013; 23:252–260. [PubMed: 23522702]
5. Mehmood S, Allison TM, Robinson CV. Annu Rev Phys Chem. 2015; 66:453–474. [PubMed: 25594852]
6. Zhou M, Jones CM, Wysocki VH. Anal Chem. 2013; 85:8262–8267. [PubMed: 23855733]
7. Breuker K, McLafferty FW. Proc Natl Acad Sci U S A. 2008; 105:18145–18152. [PubMed: 19033474]
8. Cui W, Zhang H, Blankenship RE, Gross ML. Protein Sci. 2015; 24:1325–1332. [PubMed: 26032343]
9. Lermyte F, Konijnenberg A, Williams JP, Brown JM, Valkenborg D, Sobott F. J Am Soc Mass Spectrom. 2014; 25:343–350. [PubMed: 24408179]
10. Li H, Wongkongkathep P, Van Orden S, Ogorzalek Loo R, Loo J. J Am Soc Mass Spectrom. 2014; 25:2060–2068. [PubMed: 24912433]
11. Mikhailov VA, Liko I, Mize TH, Bush MF, Benesch JLP, Robinson CV. Anal Chem. 2016; 88:7060–7067. [PubMed: 27328020]
12. Brodbelt JS. Anal Chem. 2016; 88:30–51. [PubMed: 26630359]
13. Laskin J, Futrell JH. Mass Spectrom Rev. 2005; 24:135–167. [PubMed: 15389858]
14. Xie Y, Zhang J, Yin S, Loo JA. J Am Chem Soc. 2006; 128:14432–14433. [PubMed: 17090006]
15. Adams CM, Kjeldsen F, Zubarev RA, Budnik BA, Haselmann KF. J Am Soc Mass Spectrom. 2004; 15:1087–1098. [PubMed: 15234367]
16. Yin S, Loo JA. J Am Soc Mass Spectrom. 2011; 21:899–907.
17. Zhang H, Cui W, Wen J, Blankenship RE, Gross ML. Anal Chem. 2011; 83:5598–5606. [PubMed: 21612283]
18. Li H, Wolff JJ, Van Orden SL, Loo JA. Anal Chem. 2014; 86:317–320. [PubMed: 24313806]
19. Zubarev RA, Horn DM, Fridriksson EK, Kelleher NL, Kruger NA, Lewis MA, Carpenter BK, McLafferty FW. Anal Chem. 2000; 72:563–573. [PubMed: 10695143]
20. Loo RRO, Loo JA. J Am Soc Mass Spectrom. 2016; 27:975–990. [PubMed: 27052739]
21. Shaw JB, Li W, Holden DD, Zhang Y, Griep-Raming J, Fellers RT, Early BP, Thomas PM, Kelleher NL, Brodbelt JS. J Am Chem Soc. 2013; 135:12646–12651. [PubMed: 23697802]
22. O'Brien JP, Li W, Zhang Y, Brodbelt JS. J Am Chem Soc. 2014; 136:12920–12928. [PubMed: 25148649]
23. Cammarata M, Lin KY, Pruet J, Liu HW, Brodbelt J. Anal Chem. 2014; 86:2534–2542. [PubMed: 24484264]
24. Cammarata MB, Brodbelt JS. Chem Sci. 2015; 6:1324–1333.
25. Cannon JR, Martinez-Fonts K, Robotham SA, Matouschek A, Brodbelt JS. Anal Chem. 2015; 87:1812–1820. [PubMed: 25559986]
26. Cammarata MB, Thyer R, Rosenberg J, Ellington A, Brodbelt JS. J Am Chem Soc. 2015; 137:9128–9135. [PubMed: 26125523]
27. McLuckey SA, Goeringer DE. J Mass Spectrom. 1997; 32:461–474.
28. Fung YME, Adams CM, Zubarev RA. J Am Chem Soc. 2009; 131:9977–9985. [PubMed: 19621955]
29. Hough MA, Grossmann JG, Antonyuk SV, Strange RW, Doucette PA, Rodriguez JA, Whitson LJ, Hart PJ, Hayward LJ, Valentine JS, Hasnain SS. Proc Natl Acad Sci U S A. 2004; 101:5976–5981. [PubMed: 15056757]
30. Aronsson G, Mrtensson LG, Carlsson U, Jonsson BH. Biochemistry (Mosc). 1995; 34:2153–2162.
31. Freskgård PO, Carlsson U, Mårtensson LG, Jonsson BH. FEBS Lett. 1991; 289:117–122. [PubMed: 1909971]
32. Jiang Y, Su JT, Zhang J, Wei X, Yan YB, Zhou HM. Int J Biochem Cell Biol. 2008; 40:776–788. [PubMed: 18060825]
33. Lindgren M, Svensson M, Freskgård PO, Carlsson U, Jonasson P, Mårtensson LG, Jonsson BH. Biophys J. 1995; 69:202–213. [PubMed: 7669898]

34. Liu CP, Zhou JM. Biochem Biophys Res Commun. 2004; 313:509–515. [PubMed: 14697218]
35. Carlsson U, Henderson LE, Lindskog S. Biochim Biophys Acta, Protein Struct. 1973; 310:376–387.
36. Edsall JT. Harvey Lect. 1966; 62:191–230. [PubMed: 4969961]
37. Bushmarina NA, Kuznetsova IM, Biktashev AG, Turoverov KK, Uversky VN. ChemBioChem. 2001; 2:813–821. [PubMed: 11948867]
38. Svensson M, Jonasson P, Freskgaard PO, Jonsson BH, Lindgren M, Maartensson LG, Gentile M, Boren K, Carlsson U. Biochemistry (Mosc). 1995; 34:8606–8620.
39. Banci L, Bertini I, Cramaro F, Del Conte R, Viezzoli MS. Biochemistry (Mosc). 2003; 42:9543–9553.
40. Nordlund A, Leinartaitė L, Saraboji K, Aisenbrey C, Gröbner G, Zetterström P, Danielsson J, Logan DT, Oliveberg M. Proc Natl Acad Sci U S A. 2009; 106:9667–9672. [PubMed: 19497878]
41. Rakhit R, Chakrabartty A. Biochim Biophys Acta, Mol Basis Dis. 2006; 1762:1025–1037.
42. Chan PK, Chattopadhyay M, Sharma S, Souda P, Gralla EB, Borchelt DR, Whitelegge JP, Valentine JS. Proc Natl Acad Sci U S A. 2013; 110:10934–10939. [PubMed: 23781106]
43. Morrison LJ, Brodbelt JS. J Am Chem Soc. 2016; 138:10849–10859. [PubMed: 27480400]
44. Thompson MS, Cui W, Reilly JP. Angew Chem Int Ed. 2004; 43:4791–4794.
45. Webber N, He Y, Reilly JP. J Am Soc Mass Spectrom. 2013; 25:196–203. [PubMed: 24310819]
46. Parthasarathi R, He Y, Reilly JP, Raghavachari K. J Am Chem Soc. 2010; 132:1606–1610. [PubMed: 20078132]
47. Zubarev RA. Mass Spectrometry. 2013; 2:S0004. [PubMed: 24349923]
48. Zubarev RA, Yang H. Angew Chem Int Ed. 2010; 49:1439–1441.
49. Chingin K, Makarov A, Denisov E, Rebrov O, Zubarev RA. Anal Chem. 2014; 86:372–379. [PubMed: 24236851]
50. Giuliani A, Milosavljević AR, Canon F, Nahon L. Mass Spectrom Rev. 2014; 33:424–441. [PubMed: 24375654]

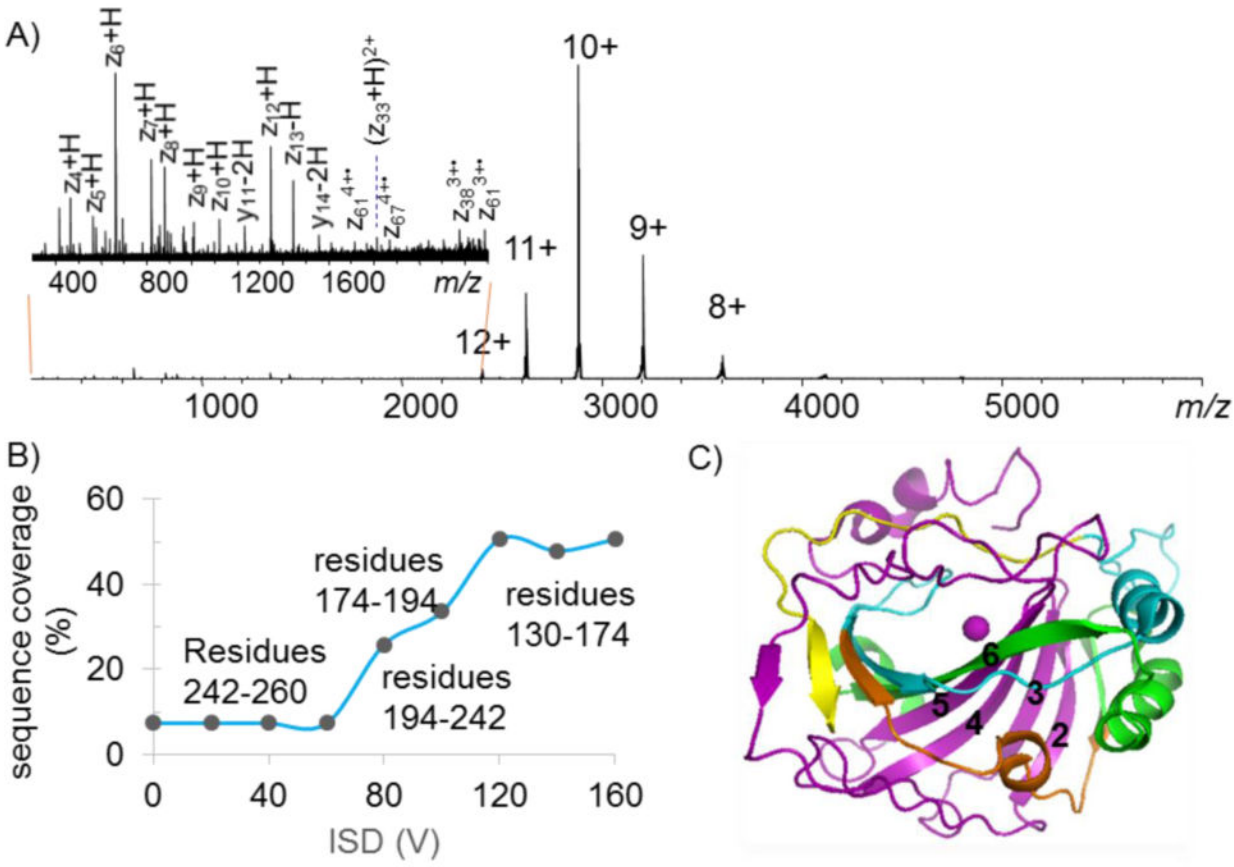

Figure 1.

(A) EID spectrum of HCA-I (9+~11+). (B) The ISD-EID sequence coverage plot of HCA-I. ISD voltage was applied to gradually unfold HCA-I before EID. The sequence coverage (%) was plotted as the y-axis and shown at the left-hand side and the corresponding unfolded sequence regions are also shown in the y-axis but displayed at the right-hand. (C) The unfolding process of HCA-I in the gas phase is shown on the X-ray structure of HCA-I (PDB 2CAB). Unfolding proceeds through the C-terminal region (residues 242-260 shown in yellow), residues 194-242 (in cyan), residues 174-194 (in orange), and to residues 130-174 (green). β-strands 2-6 compose the most stable regions of the structure.

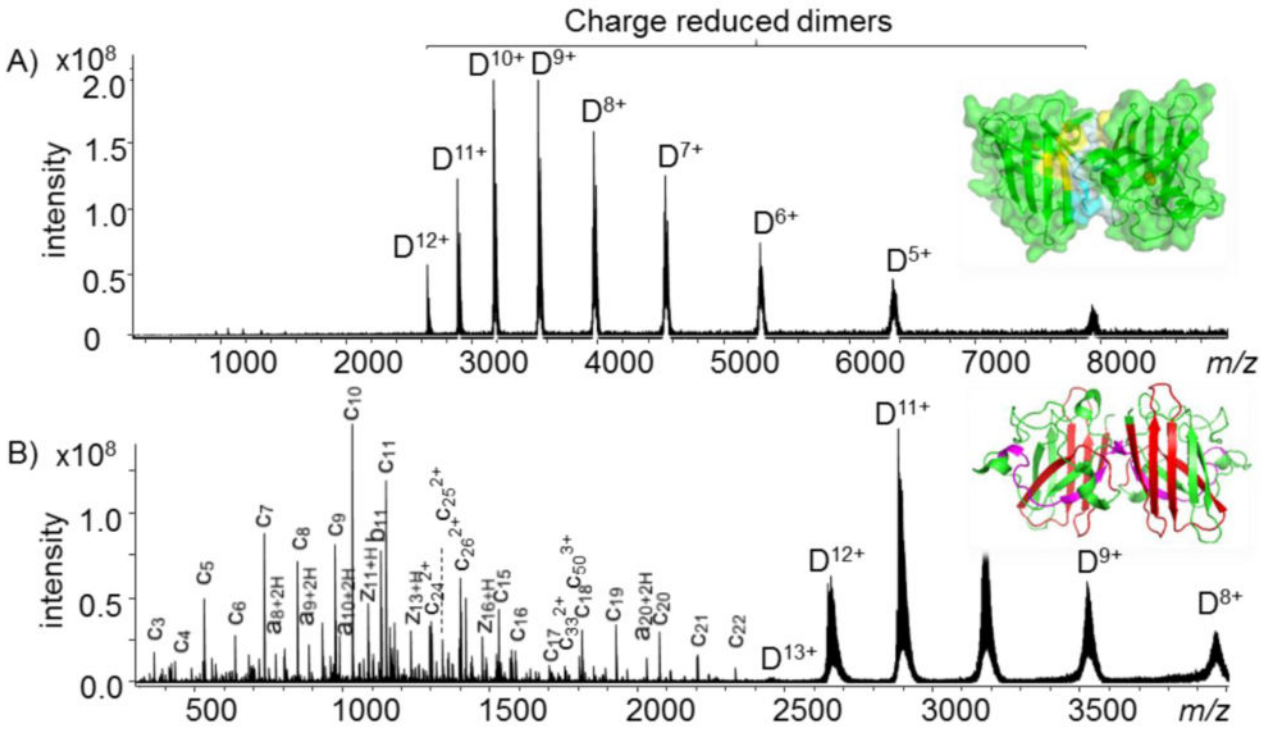

Figure 2.

Native top-down (A) ECD and (B) EID MS of the apo-SOD1 dimer (10+~12+). EID fragment ions from the N-terminal regions are color-coded in red and products from the C-terminal regions are in magenta. (Representative spectra are shown; each spectrum was acquired from 200 scans).

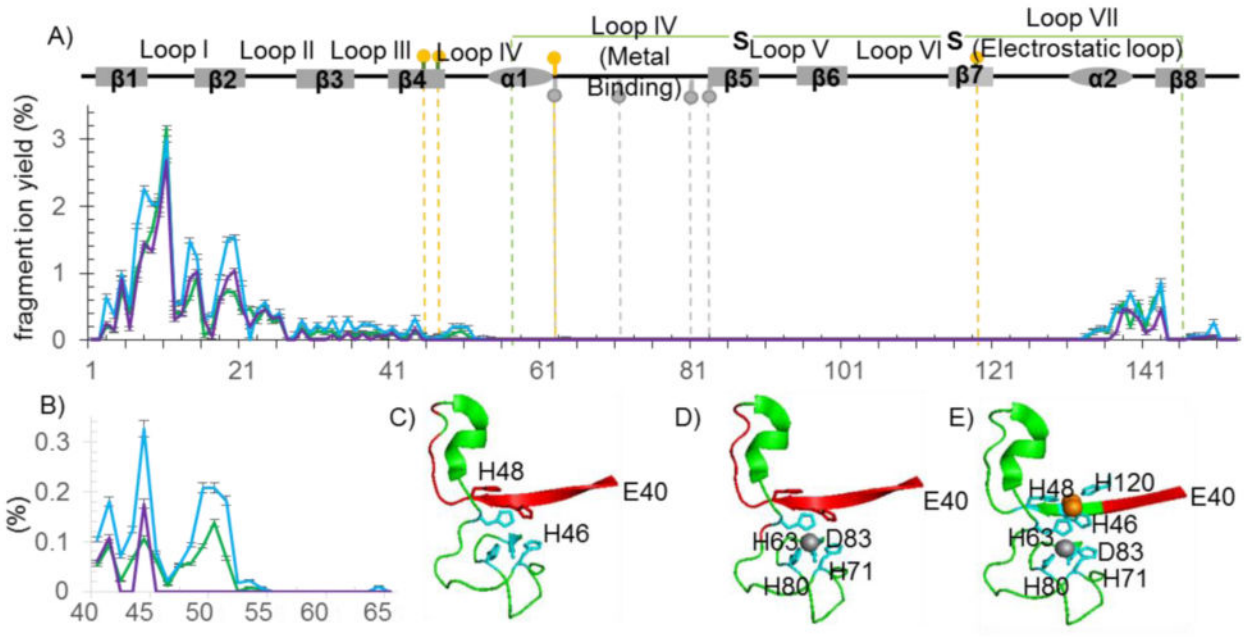

Figure 3.

(A) Plots of the EID fragment yield of SOD1 along its backbone cleavage sites (apo-WT SOD1 dimer in green, Zn-WT SOD1 in cyan, and the Cu, Zn-WT SOD1 in purple). Copper binding sites (His 46, His48, His63, and His120) are labeled in orange, zinc binding sites (His63, His71, His80, and Asp83) are in grey, and the disulfide bond (Cys57 and Cys146) is displayed in green. The secondary structure of SOD1 is shown on the top. (B) The extended region of Fig. A between residues 40-65. (C, D, and E) Partial structural region of SOD1 that displays the Zn-, Cu-bound regions and the EID fragmentation region. (C) Apo-WT SOD1, (D) Zn-WT SOD1, and (E) Cu/Zn-SOD1.

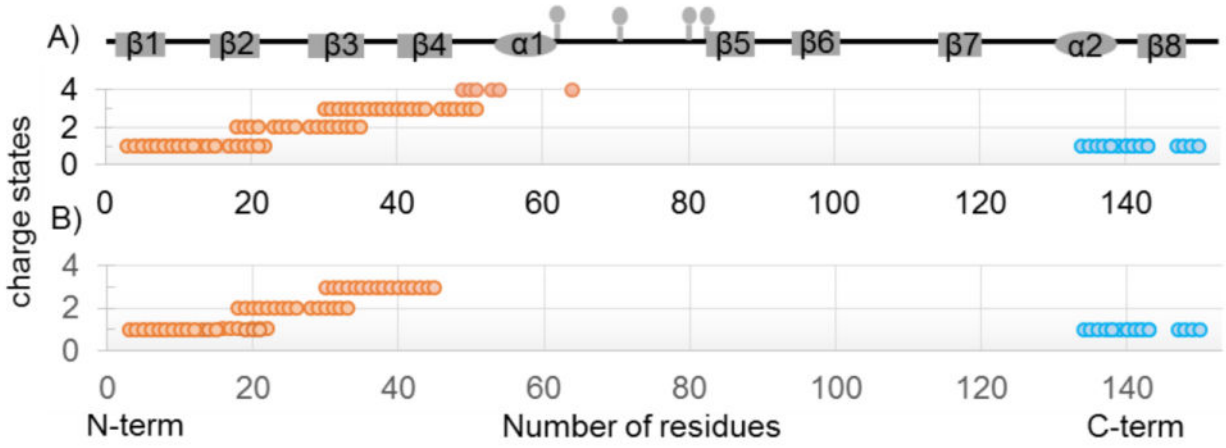

Figure 4.

Plot of backbone cleavage sites with respect to the product ion charge states for the different Zn-bound SOD1 dimers, (A) WT and (B) G41D. The fragment ions from the N-terminal region are labelled in orange dots and the fragments from the C-terminal region are in cyan dots. (Data are from representative spectra; each spectrum was acquired from 200 scans).

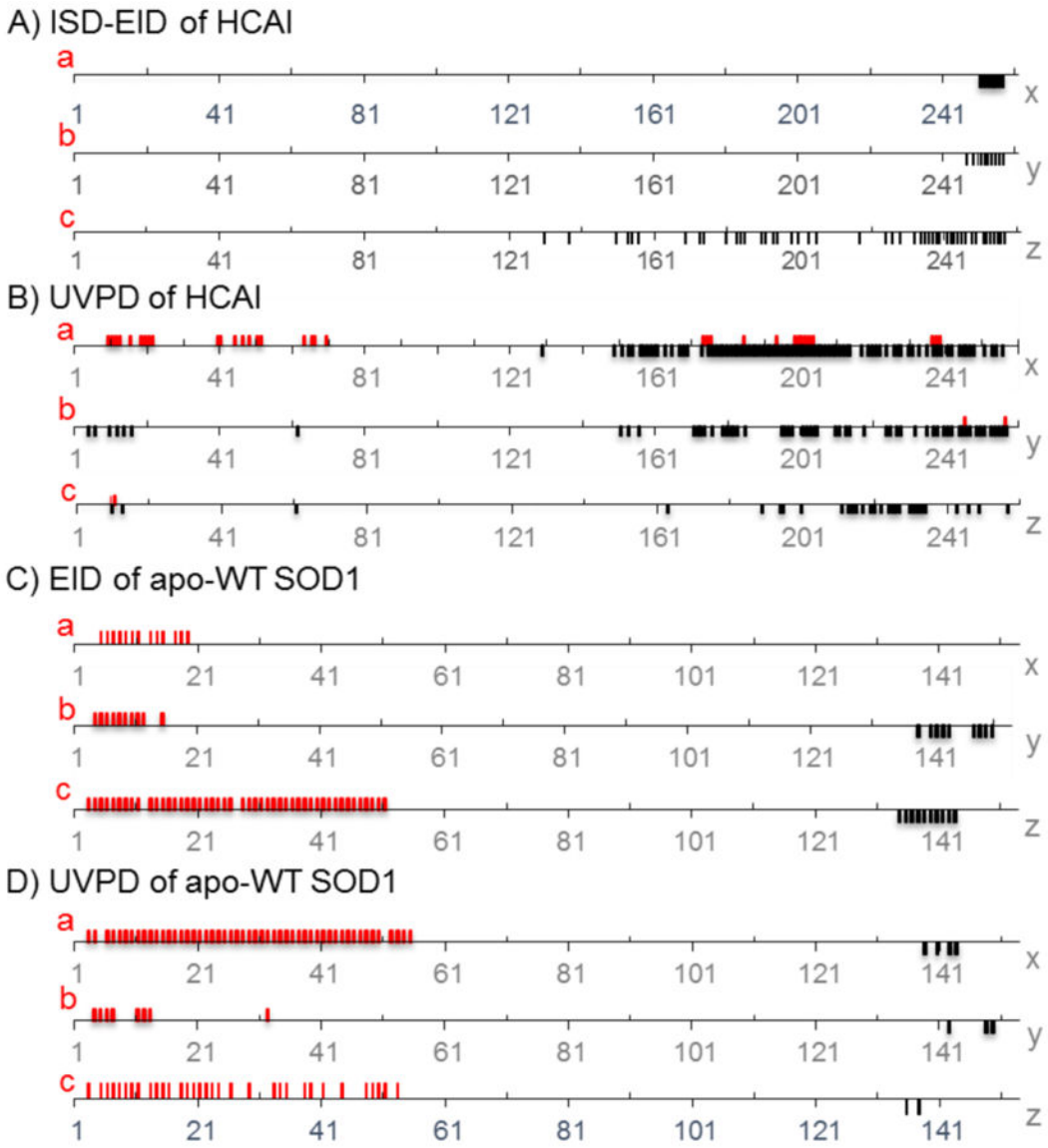

Figure 5.

Plot of backbone cleavage sites with the respect of ion-types (a/x, b/y, and c/z). (A) ISD (120V)-EID of HCA-I with a/x, b/y, and c/z ions plotted separately. (B) UVPD of HCA-I. (C) EID of apo-WT SOD1 dimer. (D) UVPD of apo-WT SOD1 dimer. (Representative spectra are shown; each spectrum was acquired from 200 scans).